An Explicit-Implicit Hybrid Solvent Model for Grand Canonical Simulations of the Electrochemical Environment

Duy Le[1,2]

[1] Department of Physics, University of Central Florida, Orlando, FL 32826

[2] Renewable Energy and Chemical Transformations Cluster, University of Central Florida, Orlando, FL 32826

Email: duy.le@ucf.edu

Abstract: The development of *ab initio* methods for atomistic simulations of the electrochemical environment is essential for obtaining a mechanistic understanding of the fundamental reactions. We propose here an explicit-implicit solvent model, SOLHYBRID, that enables grand-canonical ensemble simulations of the electrochemical environment with the popular Vienna Ab initio Simulation Package (VASP), extending its capabilities beyond the commonly used the implicit solvent model VASPSol. We further present a subroutine, TPOT, that allows control of the electrode potential, thereby enabling simulations at constant electrode potential to mimic the experimental electrochemical cell. We demonstrate the key points of our approach for the case of CO_2 adsorption on Au(110) in the presence of K^+ cation.

1 INTRODUCTION

Because of the rising demand for clean energy and CO_2 recycling, electrochemical reduction of CO_2 under ambient conditions (room temperature and atmospheric pressure) has emerged as a promising route for *hydrogen-free* sustainable fuel production, as it is compatible with the

intermittency of renewable energy sources and enables utilization of renewable electricity without the need for expansion of transmission capacity. With the development of an efficient electrochemical process for CO_2 recycling, such *clean energy* technology can ultimately close the carbon cycle for the utilization of carbon-based fuels and reduce carbon emissions to significantly mitigate the anticipated climate and environmental damage. While great progress has been made in recent times, as so well-articulated in a collection of Road Maps,[1] a number of challenges need to be overcome before controlled electrocatalytic conversion of gases such as CO_2 becomes an industrial reality.

Electrochemical reactions occur inside an environment that is complex because of the presence of multiple interfaces involving the liquid solvent, ions, gaseous reactants, and solid electrodes. To add to the complexity, the potential applied to the electrode makes the electrocatalysis process potential-dependent. Because of these heterogeneous interfaces, an atomistic understanding of the electrocatalysis process is still unclear partially because of the lack of an adequate theoretical method that incorporates the above complexities in a realistic manner.

As noted in several excellent reviews, significant advances have been made in theoretical and computational modeling of electrocatalysis.[2-4] In a nutshell, with reliance on *ab initio* techniques based on density functional theory (DFT), simulations of the electrochemical system may proceed along several strategies. The most computationally efficient approach is the implicit solvent model[5-9] in which a continuum description is applied to the electrolyte and the ions. Next are the explicit solvent models, which treat water and ions atomistically.[10] Then there is the H-shuttling method,[11-13] in which a water molecule shuttles protons to and from the electrode surface. It may also be possible to include the effect of the electrode potential in the calculations through the so-called capacitor model,[14] but such an approach fails to account accurately for the response of the

charge on the electrode to the dynamical evolution of the adsorbate, electrolyte, and the catalyst surface to keep the electrode potential constant. Fortunately, such dynamical effects are naturally included in the self-consistent grand canonical DFT (GC-DFT)[15, 16] method, but its implementation has been hampered by high computational cost. Efforts[17, 18] have also been devoted to the develop the grand-canonical AIMD (or constant potential) simulations, but so far these methods have not been widely applied.

Explicit inclusion of all components of the electrolyte, that is all water molecules, the cations, and anions, could faithfully describe the electrochemical environment. However, such a simulation with *ab initio* methods would be computationally prohibitive. In our opinion, an implicit-explicit hybrid model, in which the region near the electrode is modeled explicitly while an implicit solvent model is used elsewhere, would provide insights into electrochemical processes while keeping the computational cost manageable. In addition, such a simulation could be performed at a constant electrode potential to reflect the conditions of the "real" world electrochemical reactions.[19]

VASPSol[5, 6] is a popular implicit solvent model used for simulations of the chemistry in electrochemical environments. It treats the solvation effect via a continuum model. Intuitionally, one would think that the hybrid model mentioned above could be attained by simply adding additional explicit water molecules and ions to the simulations. Could we possibly use the implicit solvent model VASPSol as the basis for creating a hybrid solvent model?

The answer to this question is YES and NO because of the definition of the shape function,[5, 6] which is used to distinguish the solute and electrolyte in a simulation cell in VASPSol. As we explain in detail below, the shape function defines the electrolyte region through its low electron density. If the explicit solvent and ionic regions extending to a couple of angstroms from the electrode surface are pasted in VASPSol, there are regions inside the explicit electrolyte with low

or no electron density because the solvent molecules and ion do not bond to each other via covalent bonds. In VASPSol these regions will be filled with the implicit electrolyte, which would be a problem.

In this work, we propose our SOLHYBRID model which utilizes a padding charge for the explicit solvent region and an economical algorithm (TPOT) for performing simulation at a constant potential. We will also use the proposed methods to perform the *ab initio* molecular dynamics (AIMD) simulation of the adsorption of CO_2 on Au(110) surface in the presence of potassium cation (K^+) to demonstrate the viability of our proposed SOLHYBRID model and TPOT algorithm.

2 COMPUTATIONAL DETAILS

We perform density functional theory (DFT) based calculations using the VASP package[20, 21] with the implicit solvent model VASPSol,[5, 6] employing the plane-wave supercell and the projector augmented-wave methods.[22, 23] We used the generalized gradient approximation (GGA) in the form of Perdew-Burke-Ernzerhof (PBE)[24, 25] functional and the DFT-D3 van der Walls correction[26] for evaluating exchange-correlation of electrons. We set the cutoff energy for plane-wave expansion at 500 eV. We chose a Debye length of 3.04 Å, which corresponds to a bulk electrolyte concentration of 1 M, and a relative permittivity of the solvent of 78.4 (for water at the ambient condition) for all calculations with the implicit solvent model VASPSol. Our simulation supercell consists of a 5-layer, 2×3 Au(110) slab as the modeled electrode, 26 H_2O molecules, one K^+, a CO_2 molecule, and a vacuum of 15 Å to separate the periodical images along the normal direction of the electrode. We refer to this supercell as CO_2-K^+/Au(110) in what follows. We

sampled the Brillouin zone with a 3×3×1 grid and used Gaussian Smearing with $\sigma = 0.1$ eV for integration over the Brillouin zone. The threshold for convergence of electronic step is 10^{-6} eV. AIMD simulations were performed at 298.15 K in the NVT ensemble with the Nosé-Hover thermostat.[27] During the simulations, the bottom three layers of the Au electrode are held fixed. Note that the initial supercell was prepared in a way that binds CO_2 on the Au(110) surface with Au-C bond length of 2.15 Å, CO_2 bending angle ($\widehat{OCO}$) of 128.5°, above which there is a K atom with a distance of 3.58 Å to an O atom of CO_2, and 27 H_2O molecules. We performed AIMD simulations for 2 ps with low accuracy, i.e., 300 eV energy cutoff, 10^{-5} eV threshold for electronic convergence, Gamma point sampling for Brillouin zone, fixing all Au, C, and K atoms. After this step, we observed that one H_2O molecule was above all other H_2O molecules. We remove this molecule and continue the AIMD simulation for 2.5 ps. The resulting structure, after releasing the C and K atoms and atoms in the top two layers of the Au(110) slab, was the initial configuration of this work.

3 MODEL AND IMPLEMENTATION

In this section, we will introduce our hybrid solvent model, SOLHYBRID, that mitigates the issues with VASPSol in simulating the explicit solvent as discussed in the Introduction. In addition, we will present our TPOT algorithm which allows simulations at a target potential at an economical computational cost. The results of the simulations of CO_2-K^+/Au(110) system demonstrate the novelty and effectiveness of our proposed methodology.

3.1 Explicit-implicit hybrid solvent model SOLHYBRID

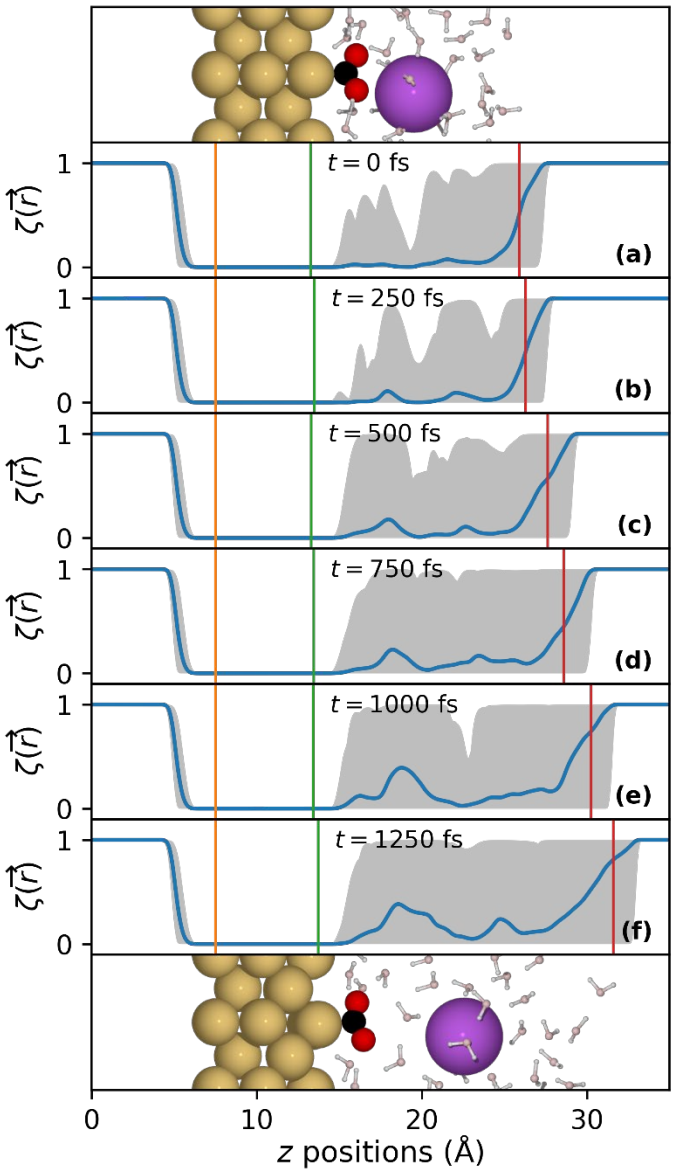

Figure 1. *Evolution of shape function (VASPSol) during AIMD simulations of CO_2-K+/Au(110). The planar average of the shape function is shown as blue lines. The shaded area indicates the range of value of the shape function. Orange, green, and red vertical lines indicate the position of the lowest Au atom, the highest Au atom, and the highest atoms of the explicit solvent molecules, respectively. The ball-stick models of the atomic configurations at 0 fs and 1250 fs are shown at the top and bottom of the figures, respectively.*

Yellow, black, red, and purple balls represent Au, C, O, and K atoms. The H_2O molecules are shown by the pink-while ball-stick molecules.

In VASPSol, the spatially dependent shape function is defined as:

$$\zeta(\vec{r}) = \frac{1}{2}\mathrm{erfc}\left\{\frac{\log[n\,(\vec{r})/n_c]}{\sigma\sqrt{2}}\right\};$$

where $n\,(\vec{r})$ is the pseudo electron density calculated as the sum of core electron density[6] $n_{core}(\vec{r})$ and valence electron density $n_{val}(\vec{r})$, at coordinate $\vec{r}$; n_c is the cutoff electron density; σ is the width of the diffuse cavity or interface region. The shape function is used to identify the region that is treated purely by DFT ($\zeta(\vec{r}) = 0$) or by implicit model ($\zeta(\vec{r}) > 0$).

With this definition, the value of shape function in the region with electron density smaller than a few n_c will be not zero and this region will be filled with explicit solvent molecules and explicit ions. **Figure 1a** shows the shape function for a hybrid solvent model, i.e., explicit H_2O and cation near the Au(110) electrode and implicit solvent elsewhere. Because of the low-density region between H_2O molecules, the value of shape function in the explicit region, between the vertical green and red lines in **Figure 1**, is not always zero. VASPsol will fill the region with implicit water molecules and ions. Since technically, the explicit water molecules and ions do not have a preference to be in either explicit or implicit regions, the explicit H_2O and ions will eventually be separated by implicit solvent. **Figure 1a-f** shows the evolution of the shape function and the structure of CO_2-K^+/Au(110) system for about 1.25 ps AIMD simulations. The range (shaded area in **Figure 1a-f**) of the shape function keeps growing and the explicit solvent layers continue to expand to fill the vacuum region. This picture is not fundamentally correct because the implicit solvent should be expelled away from the explicit region.

To mitigate the above problem, we propose our SOLHYBRID model by introducing a padding density $n_{pad}(\vec{r})$ to the pseudo electron density to ensure that the implicit solvent does not fill the explicit region. We have tried three strategies. In the first strategy, we recycled the part of the VASPSol code that calculates Gaussian core electron density $n_{core}(\vec{r})$ to calculate $n_{pad}(\vec{r})$ as the sum of Gaussian charge centered at atoms of the system, similar to the calculation of $n_{core}(\vec{r})$ but with the number of valence electrons instead of the number of core electrons and a large gaussian width. We found that strategy is not an ideal choice as the majority of the padding charge localizes at the center of each atom and that an appropriate gaussian width must be chosen to ensure that the padding charge extends to cover the space between molecules. The latter is not always satisfied because of unforeseen movements of molecules during simulations. We thus decided to remove this strategy from our implementation. The other two strategies are summarized as the two Schemes below.

Scheme 1: $n_{pad}(\vec{r})$ is the planar average of valence electron $n_{val}(\vec{r})$ which is smoothened with a Gaussian filter with a width σ_{SH} and the pseudo electron density is defined as:

$$n(\vec{r}) = n_{core}(\vec{r}) + (1 - \alpha_{SH})n_{val}(\vec{r}) + \alpha_{SH}n_{pad}(\vec{r});$$

where α_{SH} is a parameter that controls the percentage of valence density is replaced by padding density; $n_{pad}(\vec{r})$ is the planar average of $n_{val}(\vec{r})$. The optimizations of α_{SH} and σ_{SH} are necessary for building a suitable SOLHYBRID model for a specific system. In our opinion, this Scheme is the ideal one as it is calculated from the electron density of the system and has been tested to be stable during simulations.

Scheme 2: $n_{pad}(\vec{r})$ is a uniform density in the region of solute and explicit solvent and decays to zero at the interface with the implicit region and the pseudo density is defined as:

$$n(\vec{r}) = n_{core}(\vec{r}) + n_{val}(\vec{r}) + \alpha_{SH} n_{pad}(\vec{r});$$

where padding charge density $n_{pad}(\vec{r})$ is defined as $n_{pad}(\vec{r}) = \mathrm{erfc}\left\{\frac{z_{min}-z}{\sigma_{SH}\sqrt{2}}\right\} - \mathrm{erfc}\left\{\frac{z_{max}-z}{\sigma_{SH}\sqrt{2}}\right\}$; where z_{min} and z_{max} are the z coordinates of the lowest and highest points of the region where the padding charge is needed (to define the explicit solvent region). α_{SH} and σ_{SH} are parameters that control the amount of padding charge density to be added to pseudo density and the steepness of padding density near z_{min} and z_{max}. Our tests show that Scheme 2 generally works well but the choice does not reflect the electron density of a physical system. While we have implemented Scheme 2 as an option, we focused mainly on Scheme (1) and used it to produce the data presented here as our proof of concept.

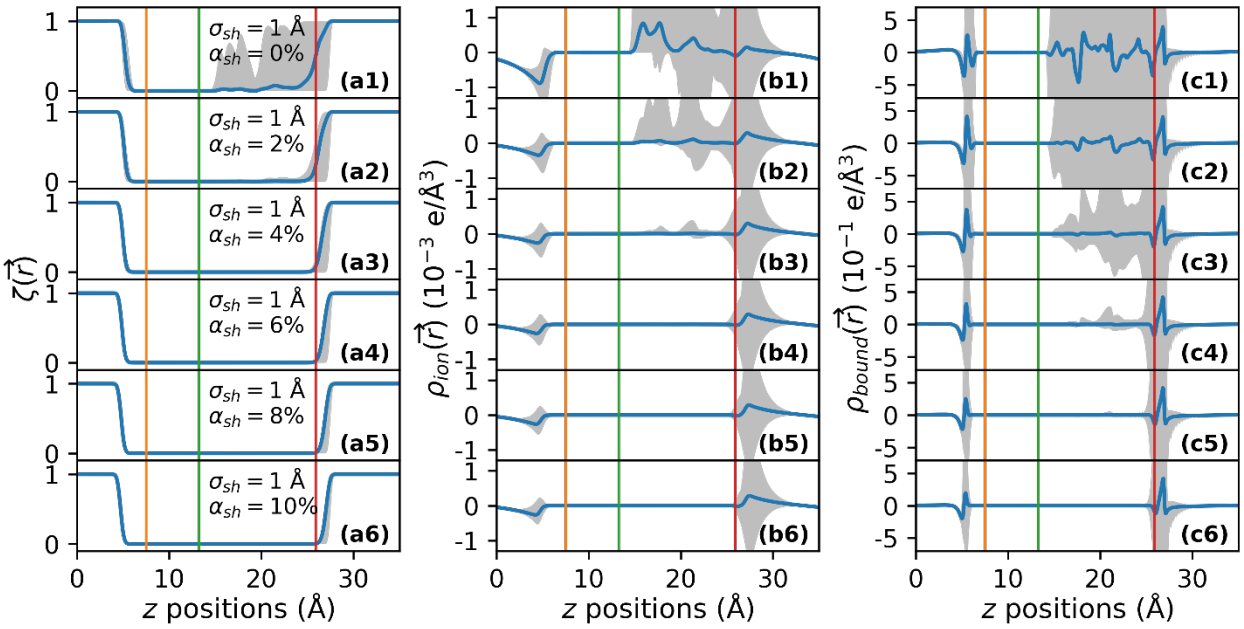

Figure 2*. The dependence of the shape function in SOLHYBRID model on* α_{SH} ***(a1-a6)*** *with* $\sigma_{SH} = 1$ Å*. Corresponding implicit ion density (*ρ_{ion}*) and bound charge density (*ρ_{bound}*) for each value of* α_{SH} *are shown in* ***(b1-b6)*** *and* ***(c1-c6)****, respectively. See* ***Figure 1****'s caption for more descriptions of lines and shaded areas.*

Figure 2(a1-a6) shows the shape function in SOLHYBRID model with $\sigma_{SH} = 1$ Å and $\alpha_{SH} = 0, 2, 4, 6, 8, 10\%$ of the same structure, CO_2-K^+/Au(111), that was used to calculate the shape function shown in **Figure 1a**. In the case of $\alpha_{SH} = 0$, the new shape function is identical to the original one, as expected. With increasing α_{SH}, the value of the shape function in the explicit region reduces (the shaded area diminished). We can achieve zero value in the explicit region with $\alpha_{SH} = 4\%$. However, our goal is not only to achieve that but also to repel implicit ion[5] and implicit bound charge[5, 28, 29] from the explicit region. We found that the implicit ion density in the explicit region approaches zero with $\alpha_{SH} = 6\%$ (**Figure 2b1-b6**) and that we can only get rid of the bound charge in explicit region with $\alpha_{SH} = 10\%$ (**Figure 2c1-c6**).

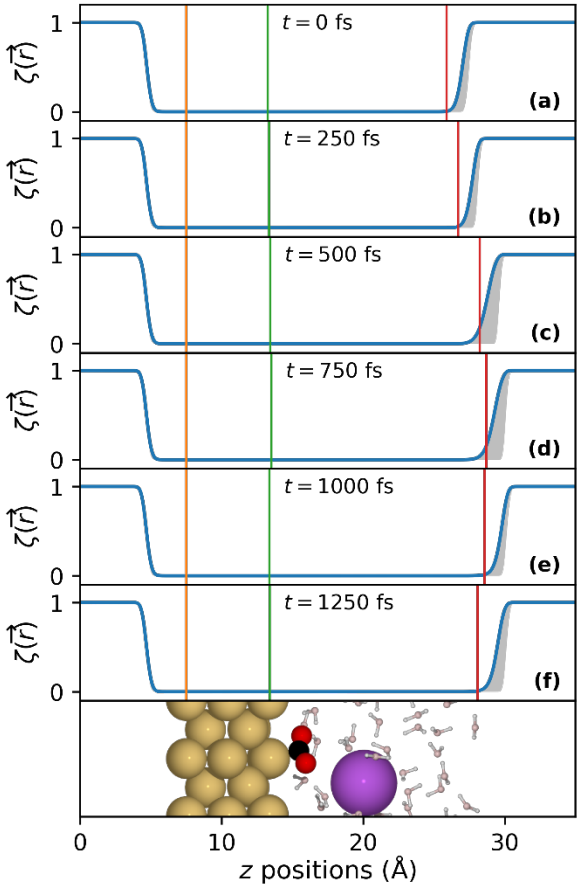

***Figure 3**. Evolution of shape function with SOLHYBRID model during AIMD simulations of CO_2-K^+/Au(110). The ball-stick model of the atomic configuration at 1250 fs is shown at the bottom of the figure. See **Figure 1**'s caption for more descriptions of lines, shaded areas, and color codes for atoms.*

We used the SOLHYBRID model with $\sigma_{SH} = 1$ Å and $\alpha_{SH} = 10\%$ to perform AIMD simulations for the CO_2-K^+/Au(110) system, with the same starting configuration of the AIMD with original VASPSol (shown in **Figure 1**). **Figure 3** summarizes the evolution of the shape function and the structure. Unlike the continuing expansion of the explicit solvent during the simulation shown in **Figure 1**, the system expands at the beginning, which is normal, and stops expanding at around 750 fs into the simulation. More importantly, values of shape function in the explicit region consistently remain zero, effectively expelling implicit solvent out of this region.

It is important to emphasize that while we discussed only the implementation of SOLHYBRID model into VASPSol, the approach, i.e., using a padding density, could also be applied to other implicit solvent models that use electron density to define the regions of solute or electrolyte, such as those implemented in ENVIRON,[8, 30-32] those originated from joint DFT framework,[33-35] SaLSA solvation model,[36] CANDLE solvation model,[7] to make them work for simulations of explicit-implicit solvents.

3.2 Controlling the electrode potential with TPOT

TPOT, **T**arget **POT**ential, is a routine that runs in conjunction with the VASP code and VASPSol to control the number of electrons during a simulation required to reach a target electrode potential. The electrode potential is defined as $\Phi = (\Phi_{Vac} - \mu_e)/\mathrm{e}$; where Φ_{Vac} is energy level at the point far away from the electrode, i.e., vacuum level, μ_e is the chemical potential of electrons, and e is the elementary charge.

In principle, the numbers of electrons can be optimized during the self-consistent field (SCF) cycles to obtain a target potential at the end of each ionic iteration.[15, 37, 38] Even though we implemented this approach in TPOT, we found that it requires substantial number of iterations and increases the computational cost.

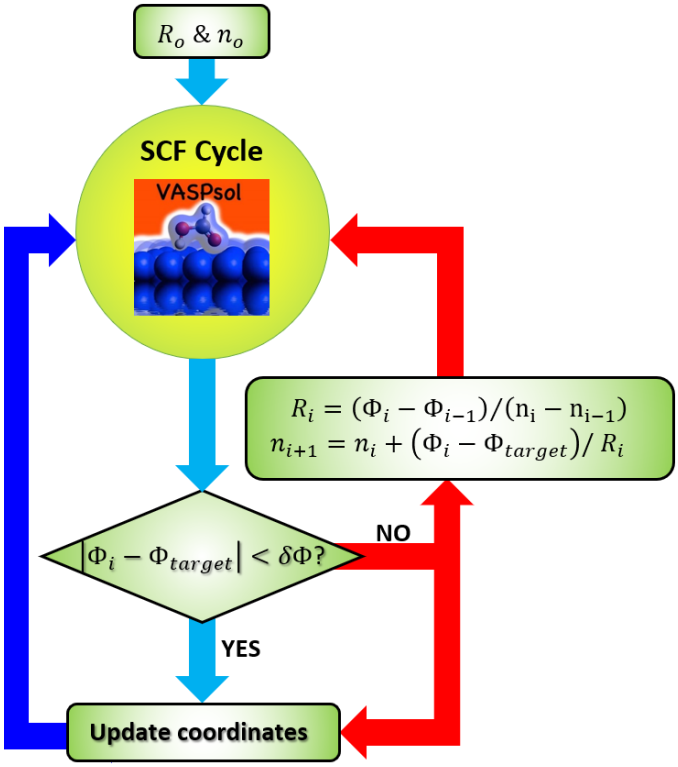

Figure 4. *Flowchart of TPOT.* R_o *and* n_o *are initial guesses of the rate of change of electrode potential with respect to the change of number of electrons and the initial number of electrons, respectively.* Φ_i, Φ_{target}, *and* $\delta\Phi$ *are electrode potential at ionic iteration* i, *target potential, and the error threshold of electrode potential.* R_i *and* n_i *are the rate of change of electrode potential and number of electrons at ionic iteration* i.

We also found that the optimization of number of electron during SCF cycle is not necessary because, during ionic relaxations or molecular dynamics simulations, the atomic structures in two consecutive steps are not substantially different, pointing to no substantial change in the electrode

potential. We, thus, propose *not to* optimize the number of electrons during SCF cycles but after each ionic iteration. The flowchart in **Figure 4** shows that TPOT needs to optimize the number of electrons only if the resulting electrode potential (Φ) differs from the target potential by an amount that is larger than a predetermined threshold $\delta\Phi$ (in practice, we set $\delta\Phi = 0.001$ V). This approach sets TPOT apart from other approaches that have been proposed[15, 37, 38] for performing constant potential calculations. It saves computational time as it requires virtually no additional cost as compared to the constant charge calculation as implemented in VASPSol.[5, 6] While, in principles, advanced methods for optimizing the number of electrons can be developed and implemented, we use a simple approach to update the number of electrons at iteration i using the following algorithm $n_{i+1} = n_i + \left(\Phi_i - \Phi_{target}\right)/R_i$ only if $\left|\Phi_i - \Phi_{target}\right| > \delta\Phi$, where $R = \partial\Phi/\partial\mathrm{n}$ is the rate of the change of electrode potential with the change in number of electrons. The rate is updated at the last time that the number of electrons is updated. R_i is calculated as $(\Phi_i - \Phi_{i-1})/(\mathrm{n_i} - \mathrm{n_{i-1}})$ or is provided as input (R_o) in first iteration.

3.3 Additional notes

During the implementation of the SOLHYBRID and TPOT, we noticed two important issues related to VASPSol that should be mentioned. The first issue is about the calculation of core electron density $n_{core}(\vec{r})$. VASPSol uses gaussian type core electrons to repel implicit solvents from the core of atoms.[6] The default value, set by VASPSol, of the number of core electrons is 0 for atoms with atomic number that is smaller than 10 and 1 otherwise. If the default values are used, some atoms will have empty cores that may be filled with the implicit solvent by VASPSol. With our SOLHYBRID model, this is not an issue as the padding charges will fill these core spaces. Nevertheless, in our modified version of VASPSol, the values of core electrons for all

species, as well as all parameters used in the model, are printed out in the main output file (i.e., OUTCAR) for alerting users. We also suggest explicitly specifying core electrons in input (i.e., INCAR) to avoid unintended outcomes.

The second issue is the calculation of the vacuum level (Φ_{Vac}). VASPSol calculated a correction for aligning the vacuum level to zero (i.e., FERMI_SHIFT).[5] This value is regarded as $-\Phi_{Vac}$.[5, 14] However, we tested and found that for charged systems, there is a small difference between FERMI_SHIFT and $-\Phi_{Vac}$. Thus, in our implementation, we calculated Φ_{Vac} from the electrostatic potential of the system. TPOT offers two options for defining electrode potential $\Phi = (\Phi_{Vac} - \mu_e)/\mathrm{e}$ and $\Phi = -(\mu_e + \mathrm{FERMI\_SHIFT})/\mathrm{e}$.

In addition, when we first realized the issue with VASPSol in simulating the explicit-implicit model, we implemented a penalty potential to prevent the explicit solvent molecules from desorbing from the explicit region. The penalty potential applied to atom I takes the form of a softplus function as $E_i^{Pen} = h_{Pen} \log\{1 + \exp[(z_i - z_o)/w_{Pen}]\}$; where z_i is the z coordinate of atom i, z_o is the center of the softplus function, h_{Pen} and w_{Pen} define the high and width of the penalty potential. We later realized that this is not a solution as it does not fix the root cause of VASPSol, i.e., the implicit solvent can fill the explicit region causing it to expand and apply stress to the electrode. We keep this implementation for rare instances in which explicit solvent molecules may desorb from the explicit region into the implicit one because in principles it should have no preference to be in either region. Note that none of the simulations presented in this paper were produced with the penalty potential described above.

4 DEMONSTRATION OF GRAND CANONICAL AIMD

In this section, we demonstrate the use of the SOLHYBRID model and TPOT for grand canonical (GC) AIMD simulations. We consider the case of CO_2 adsorption on the Au(110) electrode with the presence of one potassium cation K^+ as our toy model. We choose this particular system because it has been shown that with one K^+ the CO_2 does not stay adsorbed on the Au(110) surface during AIMD simulation with pure DFT calculations.[39]

To prepare the starting point for AIMD simulation, we first performed GC-AIMD for about 9 ps at -1 V vs RHE with the starting configuration described in Computational Details section to obtain a configuration in which CO_2 chemisorbed on the electrode, i.e., bonded to Au surface atom with $\widehat{OCO}$ bending angle that is significantly smaller than 180º, with a K^+ nearby.

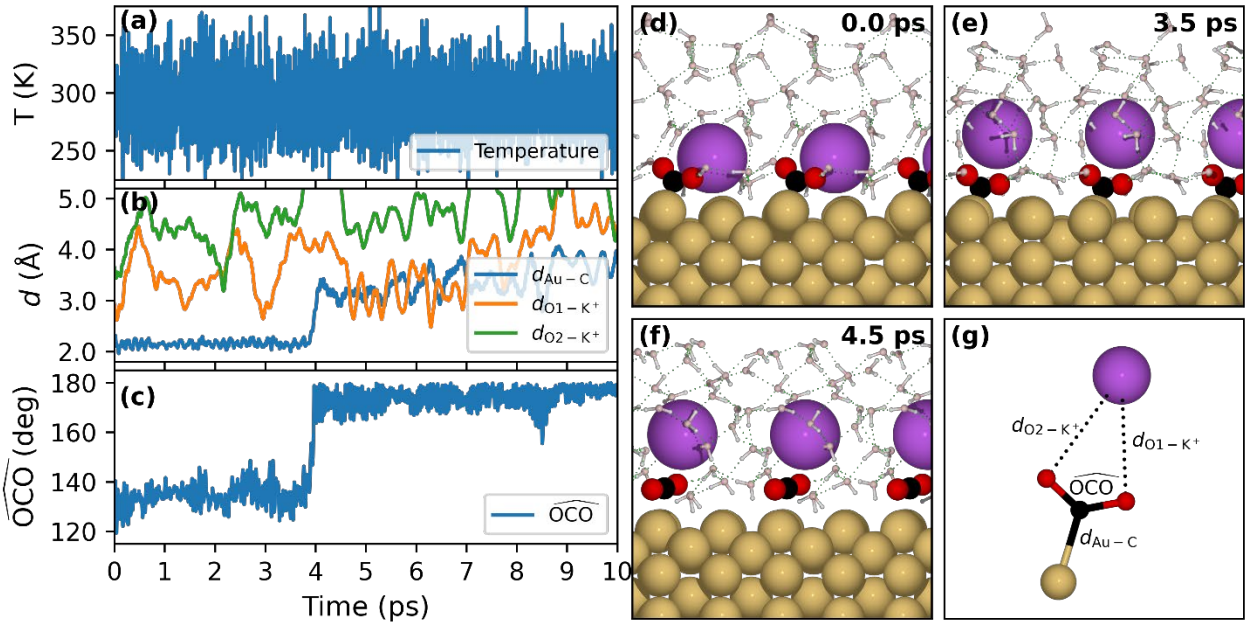

***Figure 5**. Evolution of **(a)** Temperature, **(b)** distance from Au and C atom of CO_2 molecule (d_{Au-C}), distance from K^+ to two O atoms of CO_2 molecule (d_{O1-K^+} and d_{O2-K^+}), **(c)** bending angle of the CO_2 molecule ($\widehat{OCO}$) during the AIMD simulation of CO_2-K^+/Au(111) with standard DFT. Snapshots of the*

simulations are shown in (d-f). Quantities shown in (b-c) are illustrated in ***(g)****, where all water molecules and Au atoms that are not the binding site for CO_2 were omitted for clarity. See* ***Figure 1****'s caption for the descriptions of color codes for atoms. The hydrogen bonding network is shown with green dot lines.*

Figure 5 shows the results of AIMD simulation of the system with standard DFT (PBE functional, neutral charge supercell). The movie of this simulation is provided in Supplementary Video **Movie_K+CO2_DFT.mp4**. A few snapshots of the movies are shown in **Figure 5d-f**. We found that the CO_2 chemisorbed configuration is stable on the surface for about 4 ps, after which point, the CO_2 desorbs from the surface, which is evidenced by the increase Au-C bond length from ~ 2.1 Å to > 3.0 Å (**Figure 5b**) and by the increase of $\widehat{OCO}$ angle from around or below 140° to near 180° (**Figure 5c**). The result that the CO_2 desorbs from the Au surface after a short simulation agrees with a similar simulation reported by Qin *et al*.[39]

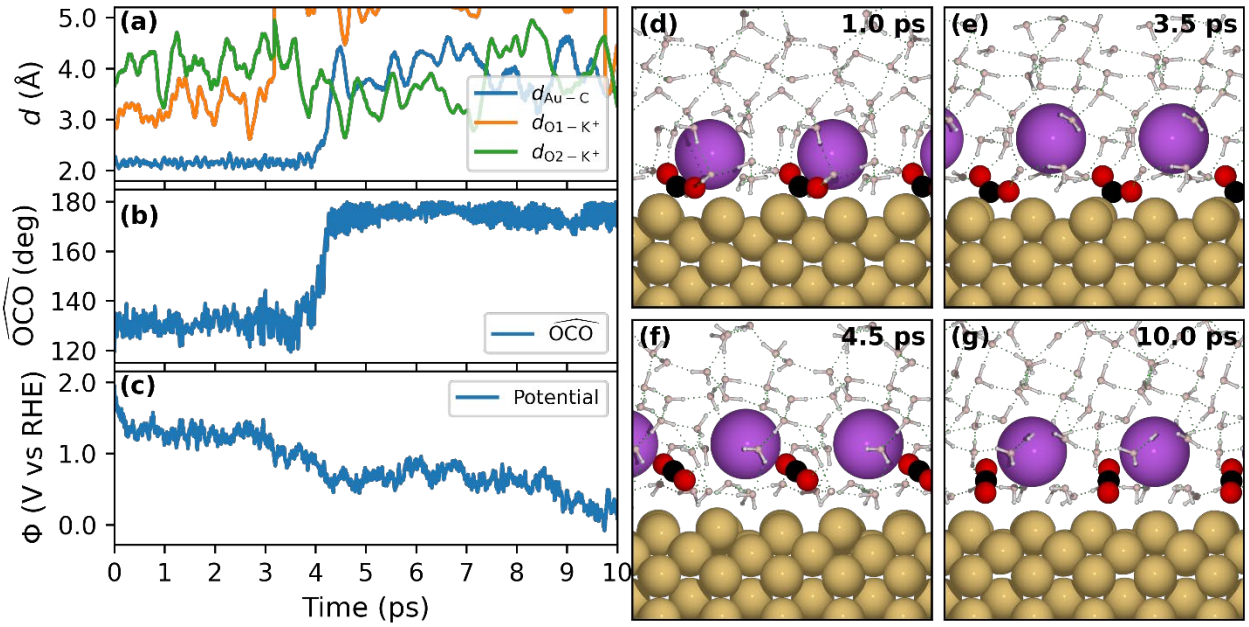

Figure 6*. Evolution of* ***(a)*** *distance from Au and C atom of CO_2 molecule (d_{Au-C}), distance from K^+ to two O atoms of CO_2 molecule (d_{O1-K^+} and d_{O2-K^+}),* ***(b)*** *bending angle of the CO_2 molecule ($\widehat{OCO}$), (c) potential of Au(110) electrode (Φ) during the AIMD simulation of CO_2-K^+/Au(111) with SOLHYBRID model.*

*Snapshots of the simulations are shown in (d-g). See **Figure 1**'s caption for the descriptions of color codes for atoms. The hydrogen bonding network is shown with green dot lines.*

We next performed a similar AIMD simulation but with SOLHYBRYD model with a neutral charge supercell. The results are summarized in **Figure 6**. The movie of this simulation is provided in Supplementary Video **Movie_K+CO2_SOLHYBRID.mp4**. A few snapshots of the movies are shown in **Figure 6d-g**. Once again, we see that the CO_2 molecule starts to desorb from the Au(110) electrode at around 4 ps second into the simulation as evidenced by the increased Au-C distance (**Figure 6a**) and $\widehat{OCO}$ angle (**Figure 6b**) in a way that is similar to AIMD simulation with standard DFT shown in **Figure 5**. The agreement between the two simulations validates our SOLHYBRID model which aims to simulate explicit solvent near the electrode surface. Thanks to our new implementation, we can calculate the electrode potential on-the-fly, as shown in **Figure 6c**. It is worth noting that the potential of the Au electrode at the beginning of the simulation is around 2 V vs RHE and decreases during the simulation to approach 0 V vs RHE at 10 ps. This variation of electrode potential is understandable because CO_2 requires electrons to be donated to its antibonding π^* orbital to form a bent configuration and to bind on the Au surface. The donated electrons are from the Au(110) surface thus increasing its electrode potential. Upon CO_2 desorption, it returns those electrons to the electrode thereby reducing its electrode potential. This behavior, i.e., variation of electrode potential, should not happen in a grand-canonical environment in which the electrode is supplied with electrons from an electron source (reservoir) during electrochemical reactions, i.e., the electrons donated to CO_2 are then replenished with electrons from the reservoir.

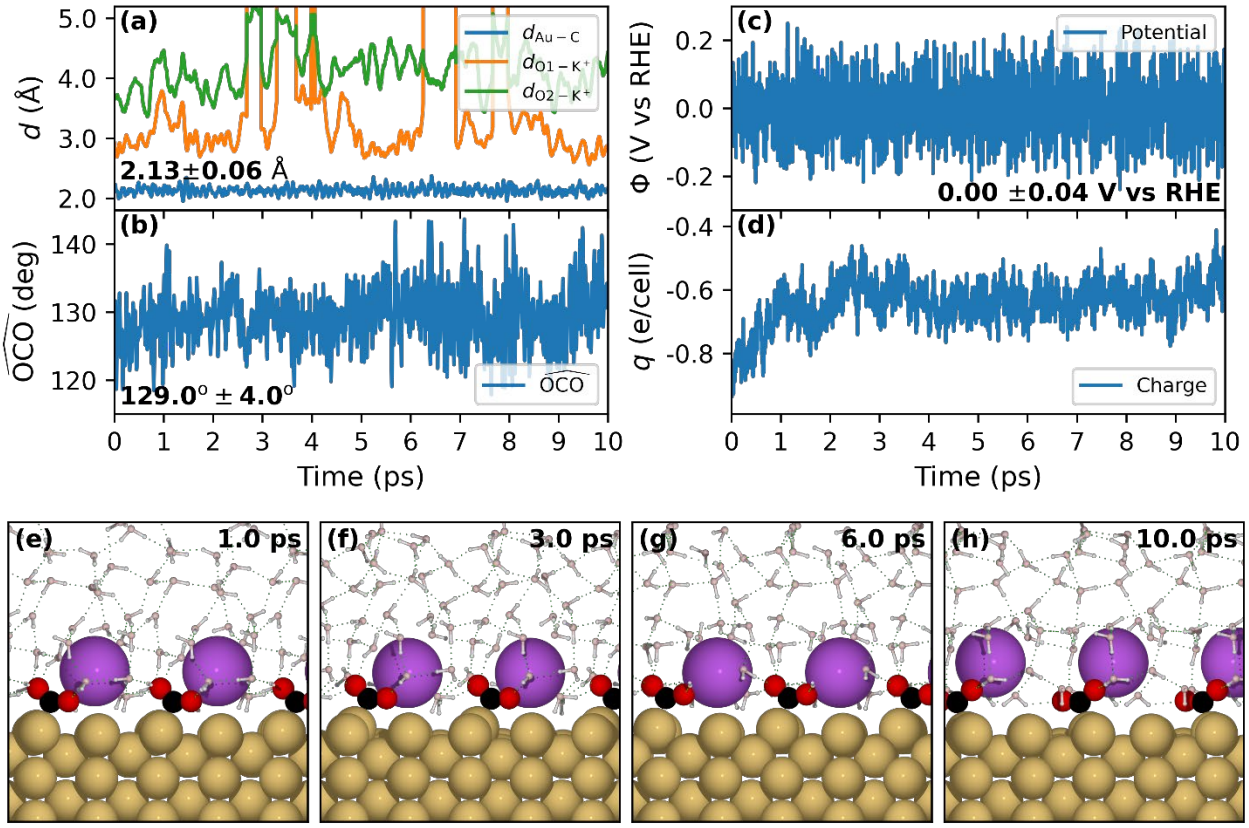

***Figure** 7. Evolution of **(a)** distance from Au and C atom of CO_2 molecule (d_{Au-C}), distance from K^+ to two O atoms of CO_2 molecule (d_{O1-K^+} and d_{O2-K^+}), **(b)** bending angle of the CO_2 molecule ($\widehat{OCO}$), **(c)** potential of Au(110) electrode (Φ), and **(d)** charge in the supercell (q) during the GC-AIMD simulation of CO_2-K^+/Au(111) with SOLHYBRID model at 0 V vs RHE. Snapshots of the simulations are shown in I-h). See **Figure 1**'s caption for the descriptions of color codes for atoms. The hydrogen bonding network is shown with green dot lines.*

We next performed GC-AIMD simulation at 0 V vs RHE. The results are summarized in **Figure 7**. The movie of this simulation is provided in Supplementary Video **Movie_K+CO2_0.0VvsRHE.mp4.** A few snapshots of the movies are shown in **Figure 7e-h**. We found that the CO_2 does not desorb from the surface during the simulation. The Au-C bond length is measured to be 2.13 ± 0.06 Å (**Figure 7a**) and the $\widehat{OCO}$ bent angle is measured to be 129° ± 4°

(**Figure 7b**). We also observed a large variation in the distance between K^+ cation and the two oxygen atoms of the CO_2 molecule. More importantly, we showed that we are able to maintain the potential of the Au electrode at 0 V vs RHE with an error of 0.04 V (**Figure 7c**). This target potential is achieved by controlling the number of electrons in the system with TPOT (**Figure 7d**).

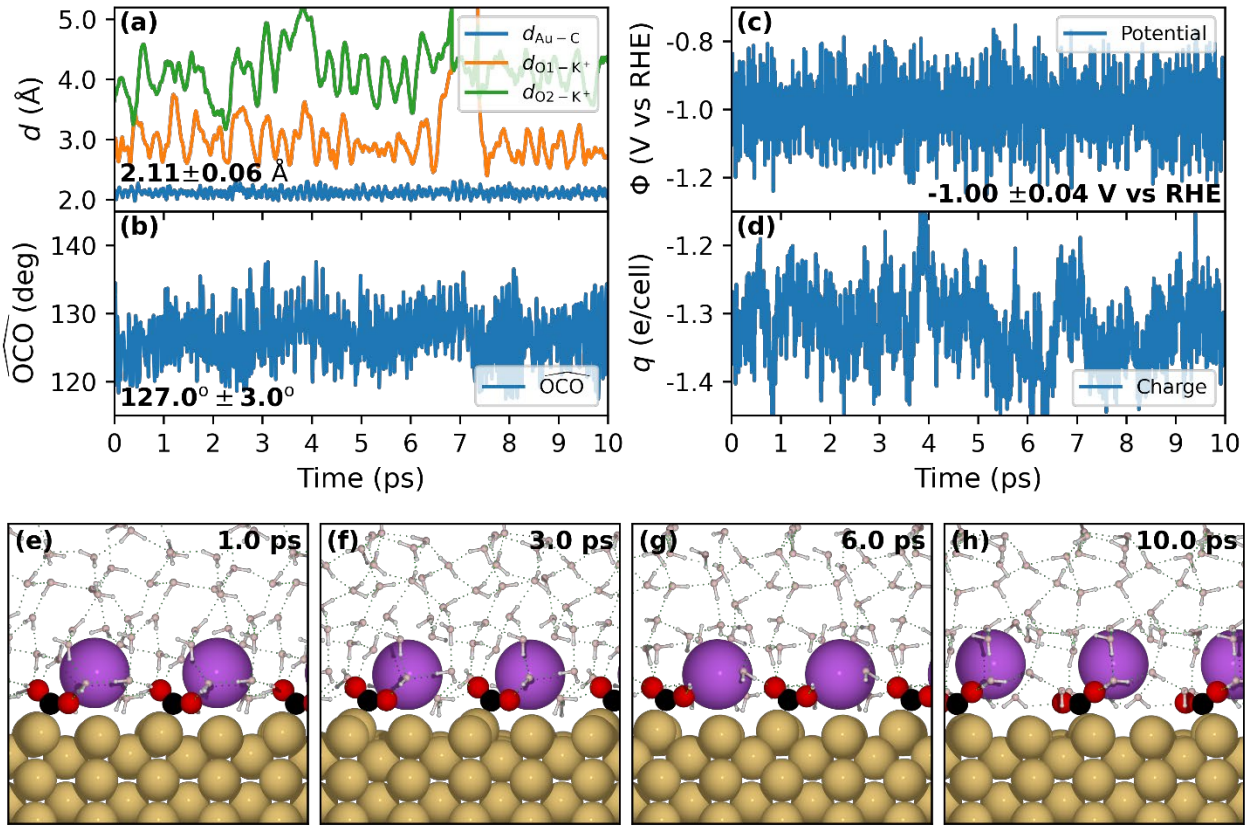

***Figure 8**. Evolution of **(a)** distance from Au and C atom of CO_2 molecule (d_{Au-C}), distance from K^+ to two O atoms of CO_2 molecule (d_{O1-K^+} and d_{O2-K^+}), **(b)** bending angle of the CO_2 molecule ($\widehat{OCO}$), **(c)** potential of Au(110) electrode (Φ), and **(d)** charge in the supercell (q) during the GC-AIMD simulation of CO_2-K^+/Au(111) with SOLHYBRID model at -1.0 V vs RHE. Snapshots of the simulations are shown iI(e-h). See **Figure 1**'s caption for the descriptions of color codes for atoms. The hydrogen bonding network is shown with green dot lines.*

Finally, we performed GC-AIMD simulation at -1.0 V vs RHE. The results are summarized in **Figure 8**. The movie of this simulation is provided in Supplementary Video **Movie_K+CO2_-1.0VvsRHE.mp4.** A few snapshots of the movies are shown in **Figure 8e-h**. We found that the CO_2 does stay adsorbed on the surface during the simulation. The Au-C bond length is measured to be 2.11 ± 0.06 Å (**Figure 8a**) and the $\widehat{OCO}$ bending angle is measured to be $127^o \pm 3^o$ (**Figure 8b**). We also observed the variations in the distance between K^+ cation and the two oxygen atoms of the CO_2 molecule are not as large as those in the simulation at 0 V vs RHE (**Figure 7a**). These results, i.e., shorter Au-C bond length, smaller $\widehat{OCO}$ angle, and smaller variations of distance from K^+ to oxygen atoms of CO_2 than those in 0 V vs RHE case, indicate that the CO_2 binds stronger on the Au(110) electrode and that the configuration and stability of the CO_2 adsorption depends on the potential of the electrode. Once again, we show that we are able to maintain the potential of the Au electrode at the target potential (-1.0 V vs RHE) with a small error of 0.04 V (**Figure 8c**). This target potential is achieved by the variation of the number of electrons in the system that is done by our TPOT algorithm (**Figure 8d**).

5 CONCLUSIONS AND OUTLOOK

In this work, we have proposed to modify the popular implicit solvent model VASPSol by using a padding charge to enable its capability to perform simulations with the explicit-implicit hybrid solvent models (SOLHYBRID) and we have introduced an economical scheme to control the electrode potential (TPOT) that optimizes the number of electrons in the system during simulation to keep the electrode at a predetermined target potential. We have also demonstrated our methods by performing (GC-)AIMD for CO_2 adsorption on Au(110) in the presence of the potassium cation.

Our approach not only allows the simulation of a hybrid explicit-implicit solvent but also facilitates the control of electrode potential with minimal error.

While we have demonstrated that the simulations (of hybrid solvent model and constant electrode potential) are feasible with the popular plane-wave DFT package, i.e., VASP, such simulations are computationally demanding mainly because of the cost associated with solving linearized Poisson-Boltzmann equation.[5] In order to use this method for realistically large length scale and long time scale simulations, it is necessary to either improve the speed of solving linearized Poisson-Boltzmann equation[5] or to use data generated from these methods to develop machine learning interaction potentials (MLIP) that are electrode-potential dependent.

Acknowledgements

We thank R. Sundararaman and T. S. Rahman for their helpful discussions and suggestions. This work is supported in part by the UCF Board of Trustee Chair Professorship awarded to T. S. Rahman. Simulations were performed using the computing resources at the Advanced Research Computing Center at University of Central Florida and the Advanced Cyberinfrastructure Coordination Ecosystem: Services & Support (ACCESS).

Data Availability

All data are included in the manuscript. Additional data supporting this work are available a zenodo repo (available at the acceptance of this manuscript) including coordinates used to generate movies, data for plotting.

Code Availability

VASP code version 5.4.4 is used for this work and is commercially available. SOLHYBRID model is implemented in our forked version of VASPSol. The code and its manual are available at https://github.com/zoowe/VASPsol. TPOT code and its manual are available at

https://github.com/zoowe/tpot. Images shown in this manuscript are generated with matplotlib, povray. Movies are created with povray and moviepy.

References:

1. I.E.L. Stephens, K. Chan, A. Bagger, S.W. Boettcher, J. Bonin, E. Boutin, A.K. Buckley, R. Buonsanti, E.R. Cave, X. Chang, S.W. Chee, A.H.M. da Silva, P. de Luna, O. Einsle, B. Endrődi, M. Escudero-Escribano, J.V. Ferreira de Araujo, M.C. Figueiredo, C. Hahn, K.U. Hansen, S. Haussener, S. Hunegnaw, Z. Huo, Y.J. Hwang, C. Janáky, B.S. Jayathilake, F. Jiao, Z.P. Jovanov, P. Karimi, M.T.M. Koper, K.P. Kuhl, W.H. Lee, Z. Liang, X. Liu, S. Ma, M. Ma, H.-S. Oh, M. Robert, B.R. Cuenya, J. Rossmeisl, C. Roy, M.P. Ryan, E.H. Sargent, P. Sebastián-Pascual, B. Seger, L. Steier, P. Strasser, A.S. Varela, R.E. Vos, X. Wang, B. Xu, H. Yadegari, and Y. Zhou, "2022 roadmap on low temperature electrochemical CO_2 reduction," Journal of Physics: Energy **4**, 042003 (2022). DOI:10.1088/2515-7655/ac7823
2. K. Chan, "A few basic concepts in electrochemical carbon dioxide reduction," Nature Communications **11**, 5954 (2020). DOI:10.1038/s41467-020-19369-6
3. G.H. Simon, C.S. Kley, and B. Roldan Cuenya, "Potential-dependent Morphology of Copper Catalysts During CO_2 Electroreduction Revealed by In Situ Atomic Force Microscopy," Angewandte Chemie International Edition DOI: 10.1002/anie.202010449 (2020). DOI:10.1002/anie.202010449
4. R. Sundararaman, D. Vigil-Fowler, and K. Schwarz, "Improving the Accuracy of Atomistic Simulations of the Electrochemical Interface," Chemical Reviews **122**, 10651-10674 (2022). DOI:10.1021/acs.chemrev.1c00800
5. K. Mathew, V.S.C. Kolluru, S. Mula, S.N. Steinmann, and R.G. Hennig, "Implicit self-consistent electrolyte model in plane-wave density-functional theory," The Journal of Chemical Physics **151**, 234101 (2019). DOI:10.1063/1.5132354
6. K. Mathew, R. Sundararaman, K. Letchworth-Weaver, T.A. Arias, and R.G. Hennig, "Implicit solvation model for density-functional study of nanocrystal surfaces and reaction pathways," Journal of Chemical Physics **140**, 084106 (2014). DOI:10.1063/1.4865107
7. R. Sundararaman and W.A. Goddard, "The charge-asymmetric nonlocally determined local-electric (CANDLE) solvation model," The Journal of Chemical Physics **142**, 064107 (2015). DOI:10.1063/1.4907731
8. O. Andreussi, I. Dabo, and N. Marzari, "Revised self-consistent continuum solvation in electronic-structure calculations," The Journal of Chemical Physics **136**, 064102 (2012). DOI:10.1063/1.3676407
9. M.M. Melander, M.J. Kuisma, T.E.K. Christensen, and K. Honkala, "Grand-canonical approach to density functional theory of electrocatalytic systems: Thermodynamics of solid-liquid interfaces at constant ion and electrode potentials," The Journal of Chemical Physics **150**, 041706 (2018). DOI:10.1063/1.5047829
10. H.H. Heenen, J.A. Gauthier, H.H. Kristoffersen, T. Ludwig, and K. Chan, "Solvation at metal/water interfaces: An ab initio molecular dynamics benchmark of common computational approaches," The Journal of Chemical Physics **152**, 144703 (2020). DOI:10.1063/1.5144912

11. X. Nie, M.R. Esopi, M.J. Janik, and A. Asthagiri, "Selectivity of CO_2 Reduction on Copper Electrodes: The Role of the Kinetics of Elementary Steps," Angewandte Chemie International Edition **52**, 2459-2462 (2013). DOI:10.1002/anie.201208320
12. X. Nie, W. Luo, M.J. Janik, and A. Asthagiri, "Reaction mechanisms of CO_2 electrochemical reduction on Cu(111) determined with density functional theory," Journal of Catalysis **312**, 108-122 (2014). DOI:10.1016/j.jcat.2014.01.013
13. W. Luo, X. Nie, M.J. Janik, and A. Asthagiri, "Facet Dependence of CO_2 Reduction Paths on Cu Electrodes," ACS Catalysis **6**, 219-229 (2016). DOI:10.1021/acscatal.5b01967
14. J.A. Gauthier, C.F. Dickens, S. Ringe, and K. Chan, "Practical Considerations for Continuum Models Applied to Surface Electrochemistry," ChemPhysChem **20**, 3074-3080 (2019). DOI:10.1002/cphc.201900536
15. R. Sundararaman, W.A. Goddard, and T.A. Arias, "Grand canonical electronic density-functional theory: Algorithms and applications to electrochemistry," The Journal of Chemical Physics **146**, 114104 (2017). DOI:10.1063/1.4978411
16. R. Sundararaman and T.A. Arias, "Joint and grand-canonical density-functional theory" in "Atomic-Scale Modelling of Electrochemical Systems". Eds. M.M. Melander, T.T. Laurila and K. Laasonen, page 139-172 (John Wiley & Sons Ltd, 2021). DOI:10.1002/9781119605652.ch4
17. F. Deißenbeck, C. Freysoldt, M. Todorova, J. Neugebauer, and S. Wippermann, "Dielectric Properties of Nanoconfined Water: A Canonical Thermopotentiostat Approach," Physical Review Letters **126**, 136803 (2021). DOI:10.1103/PhysRevLett.126.136803
18. M. Melander, T. Wu, and K. Honkala, "Constant inner potential DFT for modelling electrochemical systems under constant potential and bias," ChemRxiv (2023). DOI:10.26434/chemrxiv-2021-r621x-v3
19. D. Le and T.S. Rahman, "On the role of metal cations in CO_2 electrocatalytic reduction," Nature Catalysis **5**, 977-978 (2022). DOI:10.1038/s41929-022-00876-2
20. G. Kresse and J. Furthmuller, "Efficiency of ab-initio total energy calculations for metals and semiconductors using a plane-wave basis set," Computational Materials Science **6**, 15-50 (1996). DOI:10.1016/0927-0256(96)00008-0
21. G. Kresse and J. Furthmüller, "Efficient iterative schemes for ab initio total-energy calculations using a plane-wave basis set," Physical Review B **54**, 11169-11186 (1996). DOI:10.1103/PhysRevB.54.11169
22. P.E. Blöchl, "Projector augmented-wave method," Physical Review B **50**, 17953–17979 (1994). DOI:10.1103/PhysRevB.50.17953
23. G. Kresse and D. Joubert, "From ultrasoft pseudopotentials to the projector augmented-wave method," Physical Review B **59**, 1758–1775 (1999). DOI:10.1103/PhysRevB.59.1758
24. J.P. Perdew, K. Burke, and M. Ernzerhof, "Generalized Gradient Approximation Made Simple," Physical Review Letters **77**, 3865–3868 (1996). DOI:10.1103/PhysRevLett.77.3865
25. J.P. Perdew, K. Burke, and M. Ernzerhof, "Erratum: Generalized Gradient Approximation Made Simple," Physical Review Letters **78**, 1396 (1997). DOI:10.1103/PhysRevLett.78.1396

26. S. Grimme, J. Antony, S. Ehrlich, and H. Krieg, "A consistent and accurate ab initio parametrization of density functional dispersion correction (DFT-D) for the 94 elements H-Pu," Journal of Chemical Physics **132**, 154104 (2010). DOI:10.1063/1.3382344
27. D.J. Evans and B.L. Holian, "The Nose–Hoover thermostat," The Journal of Chemical Physics **83**, 4069-4074 (1985). DOI:10.1063/1.449071
28. S.A. Petrosyan, A.A. Rigos, and T.A. Arias, "Joint Density-Functional Theory: Ab Initio Study of Cr2O3 Surface Chemistry in Solution," The Journal of Physical Chemistry B **109**, 15436-15444 (2005). DOI:10.1021/jp044822k
29. J.-L. Fattebert and F. Gygi, "First-principles molecular dynamics simulations in a continuum solvent," International Journal of Quantum Chemistry **93**, 139-147 (2003). DOI:10.1002/qua.10548
30. P. Giannozzi, O. Andreussi, T. Brumme, O. Bunau, M.B. Nardelli, M. Calandra, R. Car, C. Cavazzoni, D. Ceresoli, M. Cococcioni, N. Colonna, I. Carnimeo, A.D. Corso, S.d. Gironcoli, P. Delugas, J. R. A. DiStasio, A. Ferretti, A. Floris, G. Fratesi, G. Fugallo, R. Gebauer, U. Gerstmann, F. Giustino, T. Gorni, J. Jia, M. Kawamura, H.Y. Ko, A. Kokalj, E. Küçükbenli, M. Lazzeri, M. Marsili, N. Marzari, F. Mauri, N.L. Nguyen, H.V. Nguyen, A. Otero-de-la-Roza, L. Paulatto, S. Poncé, D. Rocca, R. Sabatini, B. Santra, M. Schlipf, A.P. Seitsonen, A. Smogunov, I. Timrov, T. Thonhauser, P. Umari, N. Vast, X. Wu, and S. Baroni, "Advanced capabilities for materials modelling with Quantum ESPRESSO," Journal of Physics: Condensed Matter **29**, 465901 (2017). DOI:10.1088/1361-648X/aa8f79
31. G. Fisicaro, L. Genovese, O. Andreussi, S. Mandal, N.N. Nair, N. Marzari, and S. Goedecker, "Soft-Sphere Continuum Solvation in Electronic-Structure Calculations," Journal of Chemical Theory and Computation **13**, 3829-3845 (2017). DOI:10.1021/acs.jctc.7b00375
32. J.-L. Fattebert and F. Gygi, "Density functional theory for efficient ab initio molecular dynamics simulations in solution," Journal of Computational Chemistry **23**, 662-666 (2002). DOI:10.1002/jcc.10069
33. R. Sundararaman, D. Gunceler, and T.A. Arias, "Weighted-density functionals for cavity formation and dispersion energies in continuum solvation models," The Journal of Chemical Physics **141**, 134105 (2014). DOI:10.1063/1.4896827
34. D. Gunceler, K. Letchworth-Weaver, R. Sundararaman, K.A. Schwarz, and T.A. Arias, "The importance of nonlinear fluid response in joint density-functional theory studies of battery systems," Modelling and Simulation in Materials Science and Engineering **21**, 074005 (2013). DOI:10.1088/0965-0393/21/7/074005
35. K. Letchworth-Weaver and T.A. Arias, "Joint density functional theory of the electrode-electrolyte interface: Application to fixed electrode potentials, interfacial capacitances, and potentials of zero charge," Physical Review B **86**, 075140 (2012). DOI:10.1103/PhysRevB.86.075140
36. R. Sundararaman, K.A. Schwarz, K. Letchworth-Weaver, and T.A. Arias, "Spicing up continuum solvation models with SaLSA: The spherically averaged liquid susceptibility ansatz," The Journal of Chemical Physics **142**, 054102 (2015). DOI:10.1063/1.4906828
37. J.D. Goodpaster, A.T. Bell, and M. Head-Gordon, "Identification of Possible Pathways for C–C Bond Formation during Electrochemical Reduction of CO_2: New Theoretical Insights

from an Improved Electrochemical Model," The Journal of Physical Chemistry Letters **7**, 1471-1477 (2016). DOI:10.1021/acs.jpclett.6b00358

38. M.M. Melander, "Grand canonical ensemble approach to electrochemical thermodynamics, kinetics, and model Hamiltonians," Current Opinion in Electrochemistry **29**, 100749 (2021). DOI:10.1016/j.coelec.2021.100749

39. X. Qin, T. Vegge, and H.A. Hansen, "CO_2 activation at Au(110)–water interfaces: An ab initio molecular dynamics study," The Journal of Chemical Physics **155**, 134703 (2021). DOI:10.1063/5.0066196